

Doping Evolution of the Underlying Fermi Surface in  $\text{La}_{2-x}\text{Sr}_x\text{CuO}_4$ 

T. Yoshida<sup>1</sup>, X. J. Zhou<sup>2</sup>, K. Tanaka<sup>1</sup>, W. L. Yang<sup>2</sup>, Z. Hussain<sup>3</sup>, Z.-X. Shen<sup>2</sup>,  
A. Fujimori<sup>1</sup>, Seiki Komiyama<sup>4</sup>, Yoichi Ando<sup>4</sup>, H. Eisaki<sup>5</sup>, T. Kakeshita<sup>6</sup>, S. Uchida<sup>7</sup>

<sup>1</sup>Department of Complexity Science and Engineering,  
University of Tokyo, Kashiwa, Chiba 277-8561, Japan

<sup>2</sup>Department of Applied Physics and Stanford Synchrotron Radiation Laboratory, Stanford University, Stanford, CA 94305

<sup>3</sup>Advanced Light Source, Lawrence Berkeley National Lab, Berkeley, CA 94720

<sup>4</sup>Central Research Institute of Electric Power Industry, Komae, Tokyo 201-8511, Japan

<sup>5</sup>National Institute of Advanced Industrial Science and Technology, Tsukuba 305-8568, Japan

<sup>6</sup>Superconductivity Research Laboratory, ISTEK, Shinonome 1-10-13, Koto-ku, Tokyo 135-0062, Japan and

<sup>7</sup>Department of Physics, University of Tokyo, Bunkyo-ku, Tokyo 113-0033, Japan  
(Dated: October 9, 2021)

We have performed a systematic doping dependent study of  $\text{La}_{2-x}\text{Sr}_x\text{CuO}_4$  (LSCO) ( $0.03 \leq x \leq 0.3$ ) by angle-resolved photoemission spectroscopy. In the entire doping range, the underlying "Fermi surface" determined from the low energy spectral weight approximately satisfies Luttinger's theorem, even down to the lightly-doped region. This is in strong contrast to the result on  $\text{Ca}_{2-x}\text{Na}_x\text{CuO}_2\text{Cl}_2$  (Na-CCOC), which shows a strong deviation from Luttinger's theorem. The differences between LSCO and Na-CCOC are correlated with the different behaviors of the chemical potential shift and spectral weight transfer induced by hole doping.

PACS numbers: 74.25.Jb, 71.18.+y, 74.72.Dn, 79.60.-i

The pseudo-gap behavior in the underdoped high- $T_c$  cuprates has attracted significant attention and is one of the most challenging problems in strongly correlated systems. As a result of pseudo-gap opening around  $k = (\pi, 0)$ , which is observed by angle-resolved photoemission spectroscopy (ARPES) studies of underdoped cuprates [1], the electronic specific heat [2, 3, 4] and the Pauli paramagnetic susceptibility [4] decrease with decreasing hole concentration  $x$ . Such unconventional behaviors in the underdoped cuprates are thought to be a remarkable example of strong deviation from the normal Fermi liquid. However, it is still unclear whether they can be understood starting from a Fermi liquid or should be understood from a fundamentally new kind of ground state.

Theoretically, two pictures in the underdoped cuprates, namely, a large Fermi surface centered at  $(\pi, \pi)$  or a small Fermi surface centered at  $(\pi, 2\pi)$  have been considered. In theories starting from the Fermi liquid in the presence of strong antiferromagnetic fluctuations, the large Fermi surface has been obtained [5]. Uniform resonant-valence-bond (RVB) states [6], cellular dynamical mean field theory (CDMFT) [7], etc., also predict the large Fermi surface. On the other hand, flux RVB and other kinds of exotic symmetry breaking [8, 9] lead to the small Fermi surface. In the Fermi-liquid theory, the carrier number is given by the Fermi surface volume (Luttinger's theorem). However, even for the large Fermi surface, most of numerical calculations on the Hubbard and  $t$ - $J$  models have predicted noticeable deviation from Luttinger's theorem in the underdoped region that the occupied area of the Fermi surface becomes significantly larger than that expected from the hole concentration [10, 11, 12]. Since the Fermi surface and its Luttinger's theorem are at the center of the Fermi-liquid concept,

systematic experimental studies of the Fermi surface and its volume change as a function of hole doping should be crucial for understanding the ground state of the pseudo gap state in the cuprates.

Recent ARPES studies on lightly-doped cuprates [13, 14] have shown that the Fermi surface is basically large and that, while the  $(\pi, 0)$  region remains (pseudo) gapped, a quasi-particle (QP) band is formed and crosses the Fermi level ( $E_F$ ) in the nodal  $(0,0)$ - $(\pi, \pi)$  direction, leading to the picture that only part of the Fermi surface survives as an "arc" around the node. The QP crossing in lightly-doped LSCO and moderately lightly-doped Na-CCOC is certainly responsible for their metallic behavior [15]. The volume of the "Fermi surface" (which is defined under this Fermi-arc/pseudo-gap situation) in Na-CCOC was found to strongly deviate from Luttinger's theorem as the doping approaches zero [14], consistent with the theoretical predictions [10, 11, 12].

In the present study, the doping evolution of the unconventional electronic structure of LSCO with the Fermi arc and the pseudogap have been systematically studied by ARPES in the entire doping range. We have revealed the evolution of the "Fermi surface" with hole doping and found that the Fermi surface area almost fulfills Luttinger's theorem in the entire doping range even down to  $x = 0.03$ , namely, down to the "spin-glass" region. This is in strong contrast with Na-CCOC [14]. We shall discuss phenomenological as well as microscopic origins of the differences between the two systems.

The ARPES measurements were carried out at BL10.0.1 of Advanced Light Source, using incident photons of 55.5 eV. We used a Scienta SES-2002 analyzer with the total energy resolution of 20 meV and the momentum resolutions of 0.02 in units of  $1/a$ , where  $a = 3.8$

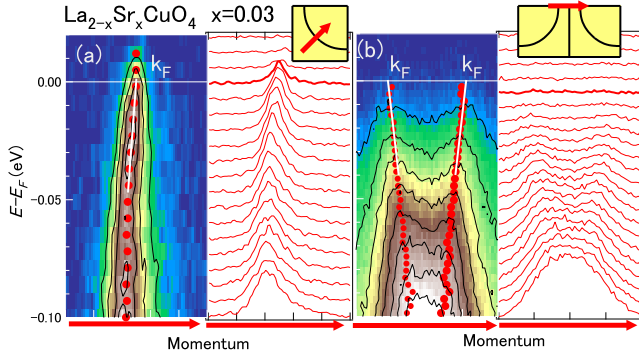


FIG. 1: (Color online) ARPES spectra of  $\text{La}_{1.97}\text{Sr}_{0.03}\text{CuO}_4$ . (a) Intensity plot in  $E$ - $k$  space (left) and MDC's (right) for the nodal cut (inset). (b) Intensity plot in  $E$ - $k$  space (left) and MDC's (right) for the anti-nodal cut near  $(\pi, 0)$  (inset). Red dots represent the peak positions in MDC's. Even in the pseudogap region near  $(\pi, 0)$ , one can determine  $k_F$  by extrapolating the MDC peaks to  $E_F$ .

$A$  is the lattice constant. High-quality single crystals of LSCO were grown by the traveling-solvent coating-zone method. The critical temperature ( $T_c$ ) of  $x = 0.07, 0.15$  and  $0.22$  samples were 14, 41 and 22 K, respectively, and  $x = 0.03$  and  $0.30$  samples were non-superconducting. The samples were cleaved in situ and measurements were performed at 20 K as in the previous studies [16]. In the present measurements, the electric vector  $E$  of the incident photons lies within the  $\text{CuO}_2$  plane, 45 degrees rotated from the  $\text{Cu-O}$  direction and is parallel to the Fermi surface segment around the diagonal region. This measurement geometry enhances dipole matrix elements in this  $k$  region because the wave function has  $x^2 - y^2$  symmetry [16].

Figure 1 shows ARPES results for LSCO ( $x = 0.03$ ), illustrating how the "Fermi surface crossing" in the pseudo-gap state can be determined from the momentum distribution curves (MDC's). In the nodal direction [(a)], where there is no gap, the underlying Fermi surface is easily determined by the MDC peak position at  $E_F$ . Near the  $(\pi, 0)$  point [(b)], on the other hand, the spectral weight is strongly suppressed due to the pseudo-gap formation. However, as shown in panel (b), one can determine  $k_F$  by extrapolating the MDC peaks up to  $E_F$  even when the spectral weight is suppressed toward  $E_F$ . Hereafter, we refer to the Fermi surface thus determined in the pseudo-gap state as the "underlying" Fermi surface. This underlying Fermi surface is consistent with the strong temperature dependence of Hall coefficient  $R_H$  [17, 18] if the low-energy spectral weight around  $(\pi, 0)$  does not contribute to charge transport at low temperatures but does at high temperatures [18].

Accordingly, we have determined the (underlying) Fermi surfaces for the entire doping range as shown in Fig. 2. Here, red dots in the momentum space indicate the  $k_F$  position of the (underlying) Fermi surface

determined using MDC's. Spectral weight at  $E_F$  is also mapped in color plot. While the optimum and overdoped samples ( $x \geq 0.15$ ) show strong intensities throughout the entire Fermi surface, the underdoped samples ( $x \leq 0.1$ ) show weak or suppressed spectral weight around  $(\pi, 0)$ , i.e., a "truncated" Fermi surface or a Fermi "arc" due to the pseudo-gap formation around  $(\pi, 0)$ . With the  $k_F$  points in the first and second Brillouin zone (BZ) as well as the shadow band in the first BZ [19], we could precisely determine the absolute momentum position of the Fermi surface for the entire doping range. From the  $E$ - $k$  space ARPES intensity plots shown in Fig. 3, one can clearly see the doping dependence of the pseudogap opening around  $(\pi, 0)$ . Although the spectral intensity at  $E_F$  around  $(\pi, 0)$  becomes weak for  $x \leq 0.15$  because of the pseudo-gap or superconducting gap opening, it is possible to identify the underlying band dispersions from the MDC peak positions (red dots) as described above. Thus, one can determine the  $k_F$  around  $(\pi, 0)$  even near the crossover from the hole-like Fermi surface to the electron-like Fermi surface.

The  $k_F$ 's determined in Figs. 2 have been fitted to the single-band tight-binding (TB) model  $\epsilon_k = \epsilon_0 - 2t(\cos k_x a + \cos k_y a) - 4t^0 \cos k_x a \cos k_y a - 2t^{00}(\cos 2k_x a + \cos 2k_y a)$ , as shown by blue curves. Here,  $t$ ,  $t^0$  and  $t^{00}$  are the first, second and third nearest neighbor transfer integrals between Cu sites. We have assumed constant  $t = 0.25$  eV and relationship  $t^{00} = t^0 = 1/2$  for all the doping levels, and regarded  $t^0$  and  $\epsilon_0$  as adjustable parameters. The fitting results of the TB parameters,  $t^0/t$  and  $\epsilon_0$  are shown in each panel of Fig. 2. Although the absolute values of  $t$ ,  $t^0$  and  $t^{00}$  are smaller than those determined by the band structure calculation by a factor of  $\sim 0.5$ , the relative magnitude of the TB parameters agree rather well with the band-structure calculation, e.g.  $t^0/t \sim 0.15$  [20]. In the overdoped region, the entire dispersion is almost perfectly fitted by the TB model, although some mismatch can be seen for the kink structure due to phonons (particularly in the nodal kink) [21, 22] and the extremely flat band dispersion around  $(\pi, 0)$  in the underdoped region. Here, the best-fit TB parameters

$t^0/t$  shown in Fig. 2 exhibit a clear doping dependence. The increase of  $t^0/t$  with decreasing  $x$  can be explained by the increase of the Cu-apical oxygen distance with decreasing  $x$  [23] according to Ref. [20]. Also, it is consistent with the CDMFT calculation [7] which indicates the increasing correlation effects in the underdoped region.

Figure 4 (a) summarizes the experimental Fermi surfaces. The hole number deduced from the area of the experimental Fermi surface,  $x_{FS}$ , obtained assuming Luttinger's theorem is plotted in Fig. 4 (b) as a function of  $x$ . It is remarkable that  $x_{FS}$  approximately accords with that predicted by Luttinger's theorem (broken lines) in the entire doping range. This result is in strong contrast with the result on Na-CCOC [14], where the  $x_{FS}$  shows a strong deviation from Luttinger's theorem in the un-

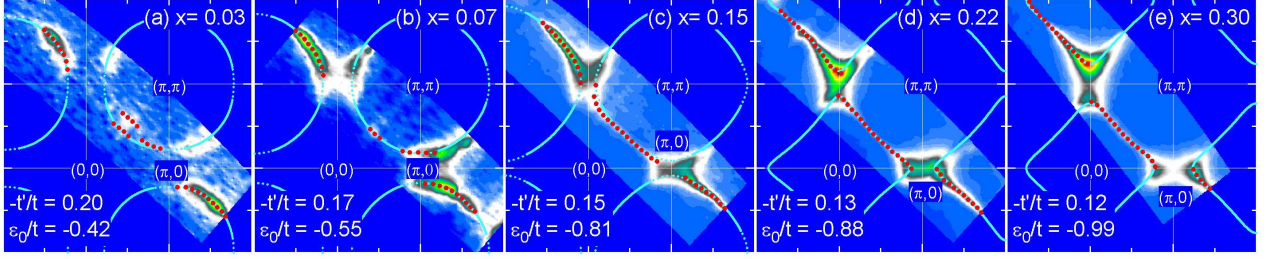


FIG. 2: (Color) Spectral weight mapping in  $k$ -space at  $E_F$  in  $\text{La}_{2-x}\text{Sr}_x\text{CuO}_4$ . Red dots indicate  $k_F$  positions determined by the MDC peaks at  $E_F$  (see Fig. 1). The blue curves show the Fermi surface interpolated by the tight-binding model.

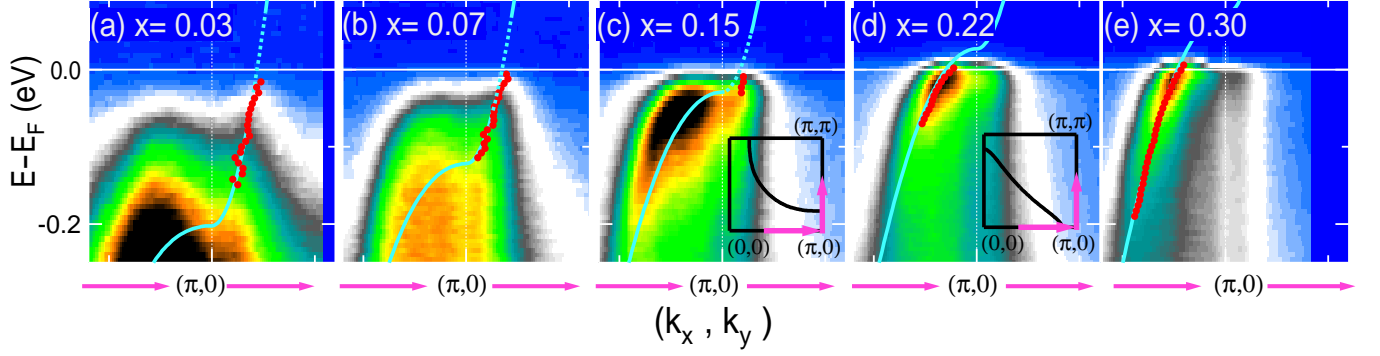


FIG. 3: (Color) Intensity plot in  $E$ - $k$  space along symmetric lines  $(0,0)$ - $(\pi,0)$ - $(\pi,\pi)$  in  $\text{La}_{2-x}\text{Sr}_x\text{CuO}_4$ . The direction and length of the arrows in the inset correspond to the horizontal axis of the color plots. The blue lines show the tight-binding interpolation. Red dots indicate MDC peaks.

deroped region, as also shown in Fig. 4(b). However, a closer inspection reveals that there may be a slight deviation from Luttinger's theorem in the lightly doped LSCO ( $x=0.03$ ) in the same direction as Na-CCOC.

In order to highlight the different shapes of the Fermi surface between LSCO and Na-CCOC, we have also plotted the doping dependence of the  $k_F$  position in the nodal direction in Fig. 4(c). Extrapolation of  $k_F$  to  $x=0$  gives  $(\pi/2, \pi/2)$  for Na-CCOC, probably reflecting the situation where the low energy excitation in the low-doping limit comes from (the tail of) the top of the lower Hubbard band (LHB), which has the band maximum at  $(\pi/2, \pi/2)$ , on the boundary of the antiferromagnetic Brillouin zone [14, 24]. In contrast, the  $k_F$  in LSCO for  $x=0.03$  is still away from  $(\pi/2, \pi/2)$ . This would be related to the observation that the spectral weight at  $E_F$  comes from the QP peak which is well separated from the LHB [13]. While the LHB in Na-CCOC approaches  $E_F$  with hole doping [24], that in LSCO stays away from  $E_F$  [13] and the spectral weight is transferred to the QP band near  $E_F$ . This contrasting behavior between LSCO and Na-CCOC is closely related to the different chemical potential shifts, that is, while photoemission spectra of Na-CCOC show rigid shifts with hole doping [24], those of LSCO show slow shifts reflecting the pinning of chemical potential at

in-gap states [25]. Although the large Fermi surface is observed in Na-CCOC, the doping evolution of the electronic structure is somewhat similar to the small Fermi surface picture in the sense that the chemical potential appears to be shifted from the top of the LHB downward. The large deviation from Luttinger's theorem may be reminiscent of the small Fermi surface behavior.

Recently, the LHB of underdoped  $\text{La}_2\text{CuO}_4$  and  $\text{Ca}_2\text{CuO}_2\text{Cl}_2$  have been interpreted as polaronic side bands [24, 26]. Although this picture well explains the LHB feature of the undoped samples, it is not straightforward to understand the different doping evolution between LSCO and Na-CCOC mentioned above. In the polaron picture, the peak of the LHB is shifted toward the  $E_F$  with hole doping since electron-phonon coupling is weakened by screening effects. However, the peak of the LHB in LSCO stays at almost the same binding energy with hole doping. This suggests that in LSCO the local charge density does not change with hole doping, reminiscent of a phase separation between hole-poor and hole-rich region. Indeed, the chemical potential pinning observed for LSCO [25] is a natural consequence of a mixture of different hole concentrations. According to a recent theoretical study, a mixed phase of antiferromagnetic (AF) and superconducting (SC) states is pro-

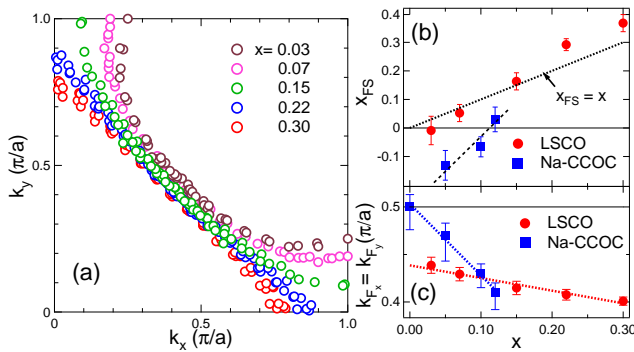


FIG. 4: (Color online) Doping dependence of the Fermi surface in LSCO. (a)  $k_F$  position for each doping determined by MDC peaks at  $E_F$ . (b) Doping dependence of the hole number  $x_{FS}$  deduced from the Fermi surface area. Luttinger's theorem  $x_{FS} = x$  is shown for comparison (broken lines). (c) Doping dependence of the  $k_F$  position in the node direction. Data for Na-CCOC [14] are also plotted.

posed to explain the coexistence of the QP states and the LHB in LSCO [27], and captures the characteristic two-component behavior of the ARPES results of underdoped LSCO [13, 28]. Also, it has been predicted that phase separation between the insulating and metallic phases occurs under a certain regime of electron-phonon coupling strength [29]. Thus, observed spectral features for LSCO are suggestive of phase separation picture. This inference is collaborated by the transport evidence for a phase separation in lightly-doped LSCO [30]. For a phase-separated state, one would normally expect to observe two Fermi surfaces corresponding the two phases. If the difference of the hole concentration between the AF and SC phases is not so large or if there are temporal fluctuations between the two phases, however, only the average of the Fermi surfaces of the two phases would be observed and would approximately fulfill Luttinger's theorem. Alternatively, the observed Fermi surface may come only from the hole-rich region. If the occupied area of the underlying Fermi surface becomes larger than that expected from the hole concentration as theoretically predicted [10, 11, 12], this effect and the increase of the hole concentration in the hole-rich region may cancel each other and Luttinger's theorem may be accidentally fulfilled.

In summary, we have observed systematic changes of the underlying Fermi surfaces in LSCO over a wide doping range. The area of the obtained underlying Fermi surface approximately satisfies Luttinger's theorem even in the lightly-doped region. This behavior is contrasted with that of Na-CCOC, which shows a clear deviation from Luttinger's theorem. Possible origins of the difference between LSCO and Na-CCOC have been discussed in relation to the chemical potential pinning and the

phase separation in the underdoped LSCO.

We are grateful to P. Pervovsek, N. Nagaosa, C. M. Ho and M. Ido for enlightening discussions. This work was supported by a Grant-in-Aid for Scientific Research in Priority Areas "Invention of Abnormal Quantum Materials", Grant-in-Aid for Young Scientists from the Ministry of Education, Science, Culture, Sports and Technology. ALS is operated by the Department of Energy's Office of Basic Energy Science, Division of Materials Science.

- [1] A. Damascelli, Z. Hussain, and Z.-X. Shen, *Rev. Mod. Phys.* **75**, 473 (2003).
- [2] J. W. Loram et al, *Physica C* **235**, 134 (1994).
- [3] N. Momono et al, *J. Phys. Soc. Jpn.* **71**, 2832 (2002).
- [4] T. Nakano et al, *Phys. Rev. B* **49**, 16000 (1994).
- [5] e.g., P. Pervovsek and A. Ramak, *Phys. Rev. B* **65** 174529 (2002).
- [6] H. Fukuyama and H. Kohno, in *Physics and Chemistry of Transition-Metal Oxides*, edited by H. Fukuyama and N. Nagaosa (Springer, Berlin, 1999), p 231.
- [7] M. Ciavelli et al, *Phys. Rev. Lett.* **95** 106402 (2005).
- [8] S. Chakravarty et al, *Phys. Rev. B* **63**, 094503 (2001).
- [9] M. E. Simon and C. M. Varma, *Phys. Rev. Lett.* **89**, 247003 (2002).
- [10] G. Esirgen et al, *Phys. Rev. B* **64**, 195105 (2001).
- [11] T. A. Maier, T. P. Ruschke and M. Jarrell, *Phys. Rev. B* **66**, 075102 (2002).
- [12] W. O. Putikka, M. U. Luchini, and R. R. P. Singh, *Phys. Rev. Lett.* **81**, 2966 (1998).
- [13] T. Yoshida et al, *Phys. Rev. Lett.* **91**, 027001 (2003).
- [14] K. M. Shen et al, *Science* **307**, 901 (2005).
- [15] Y. Ando et al, *Phys. Rev. Lett.* **87**, 017001 (2001).
- [16] T. Yoshida et al, *Phys. Rev. B* **63**, 220501(R) (2001).
- [17] H. Y. Hwang et al, *Phys. Rev. Lett.* **72**, 2636 (1994).
- [18] Y. Ando et al, *Phys. Rev. Lett.* **92**, 197001 (2004).
- [19] Because the "shadow band" is a simple replica of the main band, the origin cannot be due to antiferromagnetic fluctuations but to some extrinsic scattering effects, most likely structural defects. This issue is discussed for Bi2212 in A. Koitzsch, et al, *Phys. Rev. B* **69**, 220505(R) (2004).
- [20] E. Pavarini et al, *Phys. Rev. Lett.* **87**, 047003 (2001).
- [21] A. Lanzara et al, *Nature* **412** 510 (2001).
- [22] X.-J. Zhou et al, *Nature* **423**, 398 (2003).
- [23] P. G. Radaelli et al, *Phys. Rev. B* **49**, 4163 (1994).
- [24] K. M. Shen et al, *Phys. Rev. Lett.* **93**, 267002 (2004).
- [25] A. Ino et al, *Phys. Rev. Lett.* **79**, 2101 (1997).
- [26] O. Rosch et al, *Phys. Rev. Lett.* in press. (cond-mat/0504660).
- [27] M. Mayr, G. Alvarez, A. Moreo, and E. Dagotto, cond-mat/0503727. G. Alvarez, M. Mayr, A. Moreo, E. Dagotto, *Phys. Rev. B* **71**, 014514 (2005).
- [28] A. Ino et al, *Phys. Rev. B* **62**, 4137 (2000).
- [29] M. Capone et al, *Phys. Rev. Lett.* **92**, 106401 (2004).
- [30] Y. Ando, A. N. Lavrov, and S. Komiyama, *Phys. Rev. Lett.* **90**, 247003 (2003).